Eur. J. Mineral., 36, 209–223, 2024
https://doi.org/10.5194/ejm-36-209-2024


European Journal of Mineralogy
Open Access

Research article

# Inclusions in magmatic zircon from Slavonian mountains (eastern Croatia): anatase, kumdykolite and kokchetavite and implications for the magmatic evolution

**Petra Schneider and Dražen Balen**

Department of Geology, Faculty of Science, University of Zagreb, Zagreb, 10000, Croatia

**Correspondence:** Petra Schneider (pschneider@geol.pmf.unizg.hr)

Received: 14 July 2023 – Revised: 2 November 2023 – Accepted: 11 December 2023 – Published: 19 February 2024

**Abstract.** Micro-Raman spectroscopy was used to determine the inclusions in magmatic zircon from the Late Cretaceous A-type acid igneous rocks in the Slavonian mountains (Mt. Papuk and Mt. Požeška Gora), in the southwestern part of the Pannonian Basin (Croatia). The mineral inclusions detected in the early-crystallised zircon are anatase, apatite, hematite, ilmenite and possibly magnetite. Numerous melt inclusions comprise albite, cristobalite, hematite, kaolinite, K-feldspar, kokchetavite, kumdykolite muscovite and quartz, where this mineral association is characteristic of so-called nanorocks (nanogranites), commonly found in peritectic garnets from high-grade metamorphic rocks. Here we present the first finding of kokchetavite and kumdykolite in a magmatic zircon. Together with anatase and hematite, these polymorphs are likely evidence of rapid uplift and consequent rapid cooling of hot oxidised magma generated in the lower crust and its emplacement in the upper crustal level. This finding provides further confirmation that kumdykolite and kokchetavite do not require ultra-high pressure (UHP) to form and should not be considered exclusively UHP phases. The rapid uplift was possible due to the formation of accompanying extensional deep rifts during the tectonic transition from compression to extension, associated with the closure of the Neotethys Ocean in the area of present-day Slavonian mountains in the Late Cretaceous ( $\sim$ 82 Ma).

## 1 Introduction

Micrometre-sized inclusions are increasingly coming into scientific focus with the development of new analytical and imaging techniques that have overcome the limits of analytical resolution in the past few decades. One example is micro-Raman spectroscopy, which enables non-destructive in situ phase identification and semi-quantitative estimates of mineral composition. Studies of inclusions in general (whether mineral, melt or fluid) undoubtedly offer insights into the past of their host mineral (Ferrero and Angel, 2018). Inclusions can provide insights into the early history of the rock when enclosed in a refractory mineral such as garnet or zircon, if devoid of cracks so that the inclusion is not in contact with the rock matrix. Melt inclusions (MIs) are of particular importance as their study provides a new, unique understanding of the composition of the melt, a record that is often lost during the processes of rock crystallisation.

MIs are small droplets of melt that are trapped in minerals during their growth in the presence of a melt phase; i.e. they can be polycrystalline inclusions originally trapped as a melt but also partially crystallised inclusions or glassy ones (Sorby, 1858; Lowenstern, 2003; Thomas et al., 2003; Audétat and Lowenstern, 2014; Cesare et al., 2011, 2015). The first association of MI is obviously melt, and therefore MIs have long been studied extensively (and exclusively) in igneous rocks, especially in ore-forming systems (e.g. Sorby, 1858; Bodnar and Student, 2006; Audétat and Lowenstern, 2014). They can record initial concentrations of volatiles and metals usually lost through degassing and fractionation during magma solidification (e.g. Frezzotti, 2001), offer more detailed insight into magmatic processes (e.g. Thomas et al., 2002; Bodnar and Student, 2006), and are unaffected by subsolidus alteration as long as their host mineral remains stable (Audétat and Lowenstern, 2014).

Although zircon is widely used as a mineral tool in geology, either as a petrogenetic indicator, for geothermometry or U–Pb dating (Hoskin and Schaltegger, 2003), MI in zircon has rarely been used (Thomas et al., 2003) and has only recently come into focus (Gudelius et al., 2020; Zeng et al., 2020). Zircon is considered to be the best container for inclusions due to its stability over a wide $P$–$T$ range, its mechanical resistance, and its ubiquitous occurrence as an accessory mineral in igneous and metamorphic rocks (Harley and Kelly, 2007). Therefore, inclusions in zircon represent time capsules that are a valuable tool for constraining the magmatic history of igneous systems. In addition, MIs preserve the composition of the melt that was present during crystal growth and record the $P$–$T$ growth conditions (Audétat and Lowenstern, 2014).

In this study we present inclusions captured in magmatic zircon from the Late Cretaceous acid igneous rocks from the Slavonian mountains (Mt. Papuk and Mt. Požeška Gora) in Croatia obtained via micro-Raman spectroscopy. The discovered multiphase solid inclusions (MSIs) are interpreted as MIs. We discuss the insights they provide into the genesis of the host rock and their importance for reconstructing the early history of magma evolution in the studied area.

## 2 Geological setting

The Slavonian mountains (Croatia) in its northern part (including Mt. Papuk) are characterised by a very complex geotectonic history and record. They represent so-called *inselbergs*, surrounded by a younger (mainly Miocene) sedimentary cover of the Pannonian Basin (Fig. 1), where the pre-Variscan and Variscan rocks of the crystalline basement are exposed (e.g. Pamić and Lanphere, 1991a). This crystalline basement belongs to the Tisia Mega-Unit (Fig. 1a), a geotectonic unit regarded as a fragment that rifted and drifted from the European plate in the Middle Jurassic with the kinematically linked opening of the eastern branch of the Alpine Tethys Ocean (Schmid et al., 2008, 2020). Additionally, the southern part of the Slavonian mountains (Mt. Požeška Gora) belongs to the Sava Zone (e.g. Pamić, 2002, Fig. 1a), a suture zone formed by the collision of Europe (Tisia Mega-Unit) and Adria (Dinarides) and the closure of the Neotethys Ocean in the Late Cretaceous (Schmid et al., 2008, 2020; Ustaszewski et al., 2009). The Sava Zone is a complex belt comprising ophiolites and associated igneous, metamorphic and sedimentary rocks, including the Late Cretaceous to Early Paleogene deep-water sediments and flysch (Pamić, 1993, 2002; Pamić et al., 2002a, b).

Although Mt. Papuk is dominated by the Variscan rock complex (Tisia Mega-Unit), in its northwestern part the Late Cretaceous igneous rocks crosscut through the Variscan rock complex and cover an area of $\sim 10\,\mathrm{km}^2$ (Pamić, 1991). Together with the igneous rocks from Mt. Požeška Gora (area of $\sim 30\,\mathrm{km}^2$), they form a unique unit – the Senonian Basalt–Rhyolite Formation (SBRF; Pamić, 1997) or the Late Cretaceous bimodal volcanic association (Pamić et al., 2000). Besides basalts and rhyolites, this bimodal formation also includes granites (only at Mt. Požeška Gora) and pyroclastic material. According to previous studies (Pamić and Lanphere, 1991b; Pamić et al., 2000; Balen et al., 2020; Schneider et al., 2022), the acid varieties of SBRF have a typical A-type signature characteristic of a post-collisional, i.e. post-orogenic, setting. The geotectonic setting for the acid varieties of this formation is related to the collisional environment between the Adria Microplate and Tisia Mega-Unit, where a subducted plate (Adria) caused mantle to rise, leading to extensional rift processes in the suture zone. These local extensional zones served as pathways for the rapid ascent of hot, dry and oxidised A-type magma to the (sub)surface levels. The occurrence of this acid rock indicates the local tectonic transition from a compressional to an extensional tectonic regime at $\sim 82$ Ma (according to zircon age dating; Balen et al., 2020; Schneider et al., 2022).

## 3 Material and methods

SBRF acid rocks (rhyolites) were sampled at two localities from Mt. Papuk: Trešnjevica (sample TRES) and Rupnica (sample RUP), both geosites within the Papuk UNESCO Global Geopark (Balen et al., 2023), with the permission of the Papuk Nature Park, and one locality from Mt. Požeška Gora: rhyolite outcrop near the settlement of Vesela (sample VES) (Fig. 1b). In addition, data for granite from Mt. Požeška Gora (sample GV) from Balen et al. (2020) and preliminary results from research on rhyolite from Rupnica presented in Schneider et al. (2022) were compared and included in this study.

Zircon was extracted from the selected rock samples by a standard procedure which includes crushing the rock ($\sim 2$–$3\,\mathrm{kg}$ of each sample), sieving, heavy-liquid separation with sodium polytungstate ($\rho = 2.9\,\mathrm{g\,cm}^{-3}$), magnetic separation and handpicking. In preparation for micro-Raman spectroscopy, cathodoluminescence (CL) images of selected zircon grains were taken at (1) the Institut für Mineralogie und Kristallchemie (closed), Universität Stuttgart, with the electron probe micro-analyser (EPMA) Cameca SX100, and (2) the Department of Earth Sciences (Petrology and Geochemistry) at the University of Graz using the field emission scanning electron microscope Zeiss Gemini DSM 982.

### 3.1 Micro-Raman spectroscopy

The size of the zircon grains separated from the studied rocks is small, as they were separated from a zircon-bearing fraction of 63–32 µm, and the size of the inclusions is mostly $< 10\,\mu\mathrm{m}$. Therefore, micro-Raman spectroscopy was the best method for this study, as it additionally allows for distinguishing among different polymorphs. Analyses of the in-

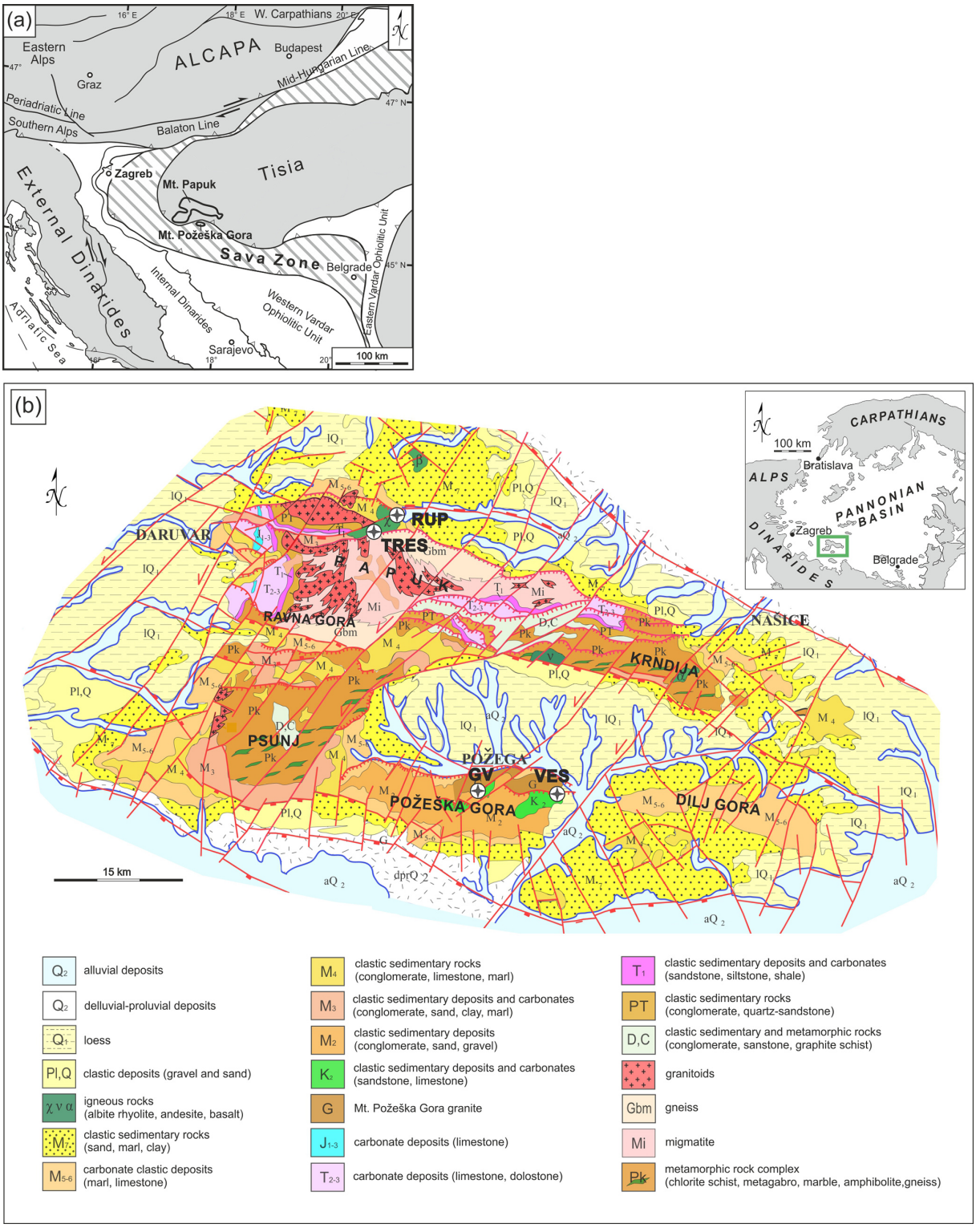


**Figure 1.** **(a)** Simplified map of the Pannonian–Carpathian–Dinaridic–Alpine region, slightly modified from Lužar-Oberiter et al. (2012), showing the major structural units according to Schmid et al. (2008). **(b)** Simplified geological map of the Slavonian mountains after Jamičić (2001, 2003) from Horvat (2004), slightly modified. The position of the sample localities are marked with stars within circles: GV – granite from Mt. Požeška Gora, RUP – Rupnica locality with rhyolite, TRES – Trešnjevica locality with rhyolite, VES – rhyolite outcrop near the settlement of Vesela. Inset shows the location of the Slavonian mountains (green rectangle) in the southwestern part of the Pannonian Basin and major mountain chains.

clusions in zircon were performed in two laboratories: (1) the Laboratory of Vibration Spectroscopy in Banská Bystrica at the Earth Science Institute of the Slovak Academy of Sciences and (2) the Department of Earth Sciences (Petrology and Geochemistry) at the University of Graz.

The working conditions were as follows: (1) a Horiba Jobin–Yvon LabRAM HR800 spectrometer equipped with a Czerny–Turner monochromator and a Peltier-cooled CCD detector coupled to an Olympus BX41 microscope with a long working distance $100\times/0.8$ objective. No special preparation was carried out prior to the analyses – the separated zircon grains were placed directly on the microscope glass slide. (2) a WITec ultra-high throughput spectrometer (UHTS) 300 SMCF VIS coupled with a confocal Raman microscope imaging system alpha3000 R equipped with a Zeiss EC Epiplan-Neofluar DIC objective lens $100\times/0.9$. Here zircon grains were handpicked, mounted in epoxy resin and polished in order to expose the interior of the grains and bring inclusions closer to the surface and thus optimise the Raman signal.

Zircon crystals were irradiated at room temperature by a He–Ne (633 nm) laser with a power of $\sim 3$ mW, and a grating of 600 grooves per millimetre was used. The Rayleigh line ($0\,cm^{-1}$) and emission bands of Ne glow lamps were used for calibration. Additionally, host zircon was used as an internal standard in every analysis. Wavenumber accuracy and lateral resolution were better than $0.8\,cm^{-1}$ and 1 µm, respectively. The spectral resolution was $\sim 3.6\,cm^{-1}$ (red spectral range). Spectra were measured with a spot size of (1) 1 µm and (2) $\sim 500$ nm. The acquisition time was 5 (number of accumulations) $\times 10$ s for each window. When zircon bands were too intensive, and therefore inclusion bands could not be distinguished in the spectra, the acquisition time was extended to up to $10 \times 20$ s per measurement. The spectra of the unknown phases were recorded in the range of 60–$4000\,cm^{-1}$ to additionally cover the region of OH-stretching bands. Only whole zircon grains or grains without visible fractures or other deformations were analysed for inclusions, proving that inclusions are isolated systems without evidence of subsequent post-entrapment re-equilibration (phase transitions). More than 300 spectra were collected. The spectra were not additionally corrected.

## 4 Results

### 4.1 Rock descriptions

At the Trešnjevica geosite the dyke swarms of various effusive rocks crosscut the older igneous rock complex and each other. Many varieties of effusive rocks include different subtypes of rhyolite, andesite, basalt, metabasalt and diabase (dolerite), but pyroclastic rocks, volcanic breccia, granite, pegmatite, gneiss and migmatite are also present on the geosite. The prevailing effusive rock is rhyolite represented with albite rhyolite, anorthoclase rhyolite and aegirine–albite rhyolite. It is light grey to greenish in colour and characterised with a porphyritic texture comprising pinkish albite phenocrysts in a fine-grained crystalised matrix composed of K-feldspar, quartz, Ti–Fe oxides and occasionally clinopyroxene (aegirine) (Fig. 2a).

The rocks at the Rupnica geosite are light grey to greenish in colour and classified as albite and aegirine–albite rhyolites. The porphyritic texture is dominated by albite phenocrysts hosted in a matrix composed of albite microliths and devitrified volcanic glass, with accessory minerals including magnetite, apatite, zircon and occasionally alkali clinopyroxene (aegirine–augite) (Fig. 2b). Detailed petrological descriptions can be found in Balen and Petrinec (2014) and Schneider et al. (2022).

The rocks from the Vesela locality are leucocratic and light grey to light brown in colour, classified as albite rhyolite. The porphyritic texture is dominated by albite phenocrysts hosted in a fine-grained crystalised matrix composed of K-feldspar and quartz (Fig. 2c). Accessory minerals include zircon, anatase and hematite.

The granite from Mt. Požeška Gora is reddish to pale pinkish in colour with a fine- to medium-grained granitic texture. It is mainly composed of alkali feldspar and quartz with minor albite (Fig. 2d). Accessory minerals include zircon, apatite, hematite and monazite. A detailed petrological description can be found in Balen et al. (2020).

### 4.2 Host zircon and inclusions

Zircon grains extracted from the samples of acid rocks (rhyolites and granites) are uniform in size and morphology among the samples, usually less than 100 µm in the longer axis, with an average aspect ratio of 2.1 : 1 (Fig. 2 insets). The grains are euhedral, with an external morphology defined by {100} prisms and {101} > {211} bipyramids. The zircon grains are colourless and highly transparent. Such features, together with the chemical composition (described in detail in Balen et al., 2020, and Schneider et al., 2022), define SBRF zircon as early-crystallised zircon (Hoskin and Schaltegger, 2003). CL images of the selected grains reveal oscillatory zoning (Fig. 3), typical of magmatic growth, without inherited or metamict cores. The inclusions are mostly less than 10–15 µm in diameter and randomly oriented with respect to the host zircon crystal growth structure (Figs. 4 and 5). They vary in shape, and some of them are euhedral and needlelike.

Raman bands of zircon (at 202, 212, 225, 356, 392, 438, 972–974 and 1005–$1008\,cm^{-1}$, the strongest at 356, 972–974 and 1005–$1008\,cm^{-1}$, after Frezzotti et al., 2012), despite the confocal mode, are very intense, occasionally making the identification of included phases difficult. The following minerals were found in inclusions: albite, anatase, apatite, cristobalite, hematite, ilmenite, kaolinite, K-feldspar, kokchetavite, kumdykolite, muscovite, quartz and possibly

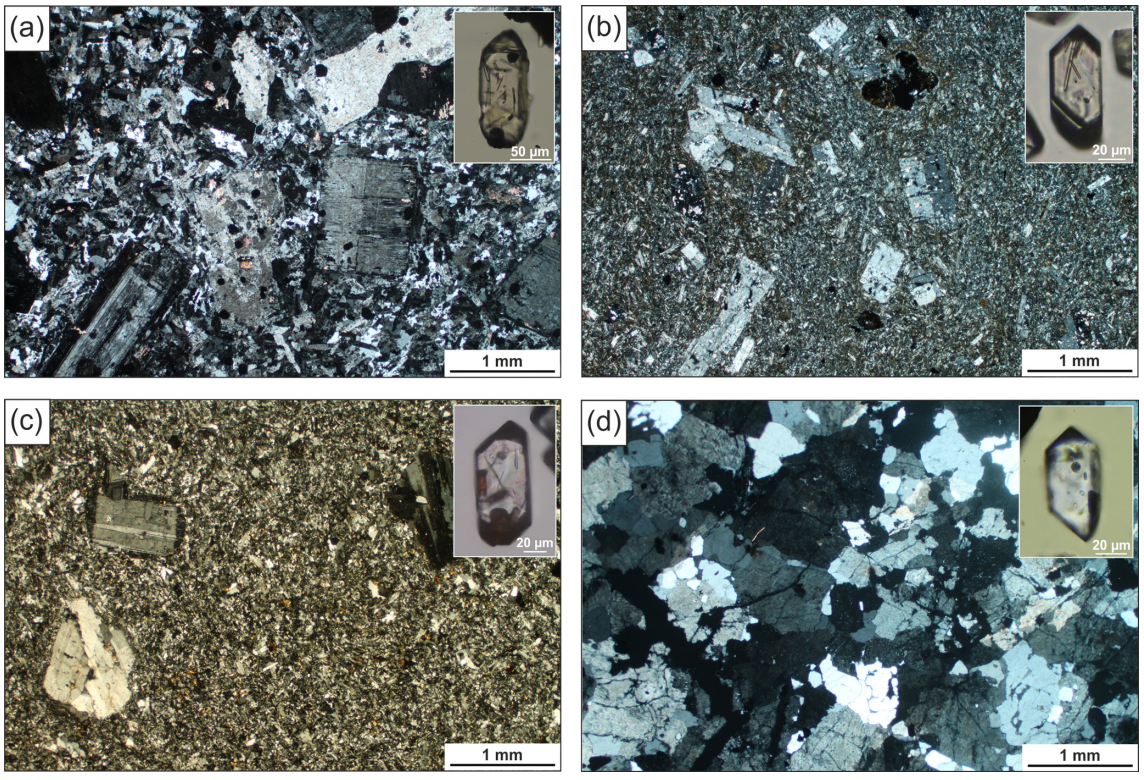


**Figure 2.** Cross-polarised transmitted-light photomicrographs of typical microfabrics for the selected SBRF rocks, with insets showing the typical morphology of zircon: **(a)** TRES rhyolite, **(b)** RUP rhyolite, **(c)** VES rhyolite, **(d)** GV granite.

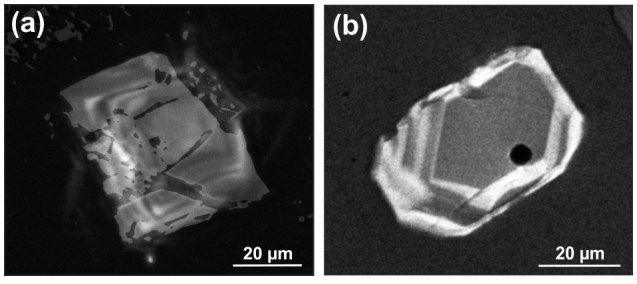


**Figure 3.** Typical CL images of magmatic zircon from acid SBRF rocks with oscillatory zoning: **(a)** section perpendicular to the *c* axis; **(b)** section along the *c* axis.

magnetite (Figs. 6 and 7). The results are summarised in Table 1, together with a list of characteristic bands for each mineral. Since the intensity of the Raman bands also depends on the orientation of the crystal lattice, the Raman bands were not always of the same intensity as those given in the reference literature, and occasionally not all bands could be detected.

The most common inclusions are colourless apatite needles (Fig. 4), which were detected in all samples and predominantly resemble spectra of fluorapatite to hydroxyfluorapatite (Fig. 6b). Hematite, a dark-coloured inclusion (sometimes distinctly red), is also detected in all samples, either as a separate solid (mineral) inclusion (Fig. 4) or within MSI (Fig. 5). Anatase, another dark-coloured inclusion, is detected in all samples, except in the TRES sample, where instead ilmenite is detected. In addition, some spectra of single mineral inclusions might correspond to magnetite (only the strongest band at 668 $cm^{-1}$ is detected, Fig. 6e).

Kumdykolite and kokchetavite are usually found together in what appears to be the same dark-coloured, brownish (and/or with a thick, dark halo) subhedral (droplet-like) or anhedral (wormlike, sometimes even amoeboid-shaped) MSI, often attached to apatite needles (Fig. 5c) and frequently accompanied by very fine red hematite crystals (Fig. 7b). Within some larger MSIs ($\sim$ 20 µm), smaller daughter crystals can be recognised (Fig. 7a). Additionally, some MSI spectra correspond to muscovite (Fig. 7c, d), albite (Fig. 7e), K-feldspar (Fig. 7f), quartz (Fig. 7f) and cristobalite (Fig. 7g). In a few MSIs from the VES sample, kaolinite is also detected (Fig. 7h).

## 5 Discussion

MIs in igneous rocks have been studied for a long time but not so extensively in magmatic zircon, which has only recently come into focus (e.g. Gudelius et al., 2020; Zeng et al., 2020). Here we report MSIs in magmatic zircon

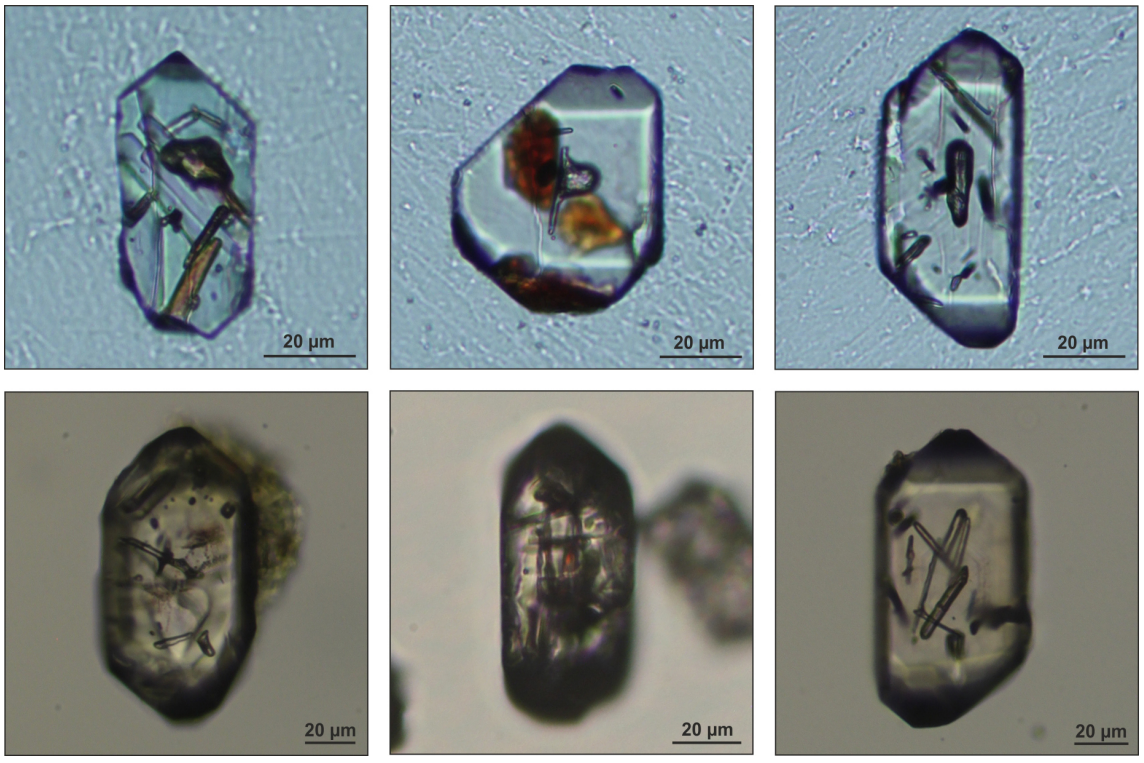


**Figure 4.** Separated zircon grains typical for acid SBRF rocks with an abundance of inclusions: colourless needles of apatite, dark-coloured inclusions of oxides (anatase, hematite and magnetite) where hematite is distinctly red, and MI in the form of bubbles or anhedral yellowish to brown inclusions with a dark halo.

with the association of feldspar polymorphs (kumdykolite, kokchetavite, albite and/or K-feldspar), $SiO_2$ polymorphs (quartz or cristobalite), OH-bearing phases (phyllosilicates – muscovite and kaolinite) and hematite. Such mineral association confirms the existence of granitic melt, proving that MSIs are indeed crystallised melt and therefore can be regarded as MIs (e.g. Ferrero and Angel, 2018). Crystallised MIs detected in acid SBRF rocks are identical to those reported in migmatites, initially found having a granitic s.l. composition, representing so-called nanogranites (Cesare et al. 2009), i.e. nanogranitoids (Cesare et al., 2015). MIs were later shown to have a more diverse composition from silicatic to carbonatitic and were therefore named nanorocks (Bartoli and Cesare, 2020). MIs and nanorocks have lately become a matter of considerable scientific interest in the reconstruction of metamorphic processes (e.g. Cesare et al., 2009, 2015; Nicoli and Ferrero, 2021). Besides the information on the history of the host mineral and/or host rock, they additionally widen the horizons of crustal petrology, helping us to understand crustal differentiation, the mechanisms and nature of crustal melting, the formation and differentiation of the early continental crust, etc. (Cesare et al., 2015). As recently suggested, anatectic MI could help constrain the crustal component of the volatile cycle, with melt and fluid inclusions in metamorphic crustal rocks representing a remarkable record that allows quantifying even the evolution of plate tectonics (Nicoli and Ferrero, 2021). However, in previous studies nanogranitoids have always been reported in partially melted rocks (see Bartoli and Cesare (2020) for a detailed overview), where they represent the products of melting reaction, i.e. anatectic melts, while here in magmatic zircon nanogranitoids represent enclosed pockets of a parental melt.

Crystallised MIs often appear brownish when observed with an optical microscope (Ferrero et al., 2012; Cesare et al., 2015) and as melt pockets attached to mineral inclusions (most commonly apatite needles, Gudelius et al., 2020; but also rutile, Ferrero et al., 2012), which corresponds to the appearance of the MSIs observed here (Fig. 5).

Although not previously reported in the MIs, kaolinite could form as an alteration product of feldspar(s) due to $H_2O$ released during crystallisation of the melt but trapped in a closed system of MIs (Silvio Ferrero, personal communication, 2023). The phyllosilicates (muscovite and kaolinite) detected in MIs confirm the presence of $H_2O$ in the originally trapped melt. In addition to MSIs, i.e. MIs, single inclusions of apatite, anatase, ilmenite, hematite and possibly magnetite are present in magmatic zircon.

**Table 1.** Summarised results of the inclusion study on selected acid rocks from the SBRF with a list of the Raman bands typical of each mineral and the reference literature. The strongest bands are in bold. Data for granite from Mt. Požeška Gora (GV) are from Balen et al. (2020).

| Mineral | Raman bands ($cm^{-1}$) | References | Mt. Požeška Gora | | Mt. Papuk | | *n* |
|---|---|---|---|---|---|---|---|
| | | | GV | VES | RUP | TRES | |
| Albite (Ab) | 163, 183, 210, 251, **292**, 328, 457, 480, **508**, 764, 816, 977, 1032, 1098 | Frezzotti et al. (2012) RRUFF (2023a) | | x | | x | 9 |
| Anatase (Ant) | **143**, 195, 395, 514, **638** | Frezzotti et al. (2012) | x | x | x | x? | 11 |
| Apatite (Ap) (FOH) | 432, 449, 581, 592, 608, **965**, 1042, 1053, 1081, 3537, 3573 | Penel et al. (1997) | x | x | x | x | 78 |
| Cristobalite (Crs) | 114, 230, 273, 286, **420**, 792, 1075 | Frezzotti et al. (2012) RRUFF (2023b) | | | | x | 1 |
| Hematite (Hem) | 144, 223, **290**, **409**, 498, 609, 1313 | Frezzotti et al. (2012) RRUFF (2023c) | x | x | x | x | 39 |
| Ilmenite (Ilm) | 232, 373, **685** | Frezzotti et al. (2012) RRUFF (2023d) | | | | x | 8 |
| Kaolinite (Kln) | **131**, 141, 197, 248, **270**, 335, 396-430, **463**, 509, 655, 700, **750**, 790, 915, 936, 1043, 1110, 3691, 3650, 3667, 3686, 3695 | Kloprogge (2017) | | x | | | 2 |
| K-feldspar (K-Fsp) | 108, 127, 159, 178, 199, 263, 267, 286, 455, **475**, **514**, 651, 749, 813, 1007, 1128, 1142 | Frezzotti et al. (2012) RRUFF (2023e) | | x | | x | 7 |
| Kokchetavite (Kct) | 110, **391**, **835** | Kanzaki et al. (2012) | x | x | x? | x | 26 |
| Kumdykolite (Kdy) | 154, **222**, 265, 407, 464, **492** | Kotková et al. (2014) | x | x | x? | x | 32 |
| Magnetite (Mag) | 193, 306, 538, **668** | Frezzotti et al. (2012) | | x? | x? | x? | 5 |
| Muscovite (Ms) | 178, 197, 216, **261**, 385, 407, 639, **702**, 754, 914, 957, 1117, **3627** | Frezzotti et al. (2012) | | x | | x? | 18 |
| Quartz (Qz) | **128**, **206**, 265, 356, 402, **464**, 698, 1161 | Frezzotti et al. (2012) RRUFF (2023f) | x | x | | x | 8 |

*n* – number of spectra where the phase was identified; x – confirmed; x? – possible finding (not all characteristic bands were detected).

### 5.1 Kumdykolite and kokchetavite

Kumdykolite is an orthorhombic polymorph of albite ($NaAlSi_3O_8$). The first finding of this polymorph was documented by Hwang et al. (2009), where kumdykolite was found in the Kokchetav ultra-high-pressure (UHP) massif in Kazakhstan as micrometre-scale (1–5 µm) crystals in MSIs (together with diopside, cristobalite/quartz, phyllosilicates, amphibole and/or carbonates) in omphacite of eclogite. It was presumed that kumdykolite, formed under high temperatures with rapid cooling and in the absence of water, represents evidence of the UHP conditions. Németh et al. (2013) documented kumdykolite in a porous silica core of a concentrically zoned metal–sulfide nodule in a meteorite, assuming that kumdykolite did not form at high pressure but rather under high temperature, presumably $> 1300$ K. Kumdykolite was also documented in an MSI (together with phlogopite and quartz) within garnet in a UHP diamond-bearing quartzofeldspathic granulite, from the northern Bohemian Massif (Kotková et al., 2014), and further in felsic granulites in the Moldanubian Zone of the Bohemian Massif, as a part of MSIs in garnet and zircon (Perraki and Faryad, 2014).

Kokchetavite is a hexagonal polymorph of K-feldspar ($KAlSi_3O_8$), first observed by Thompson et al. (1998) in experiments with synthetic starting materials as a "hexasanidine", a product of dewatering of "sanidine hydrate" (K-cymrite, another metastable polymorph and a hydrated form of K-feldspar, $KAlSi_3O_8 \cdot nH_2O$; Seki and Kennedy, 1964).

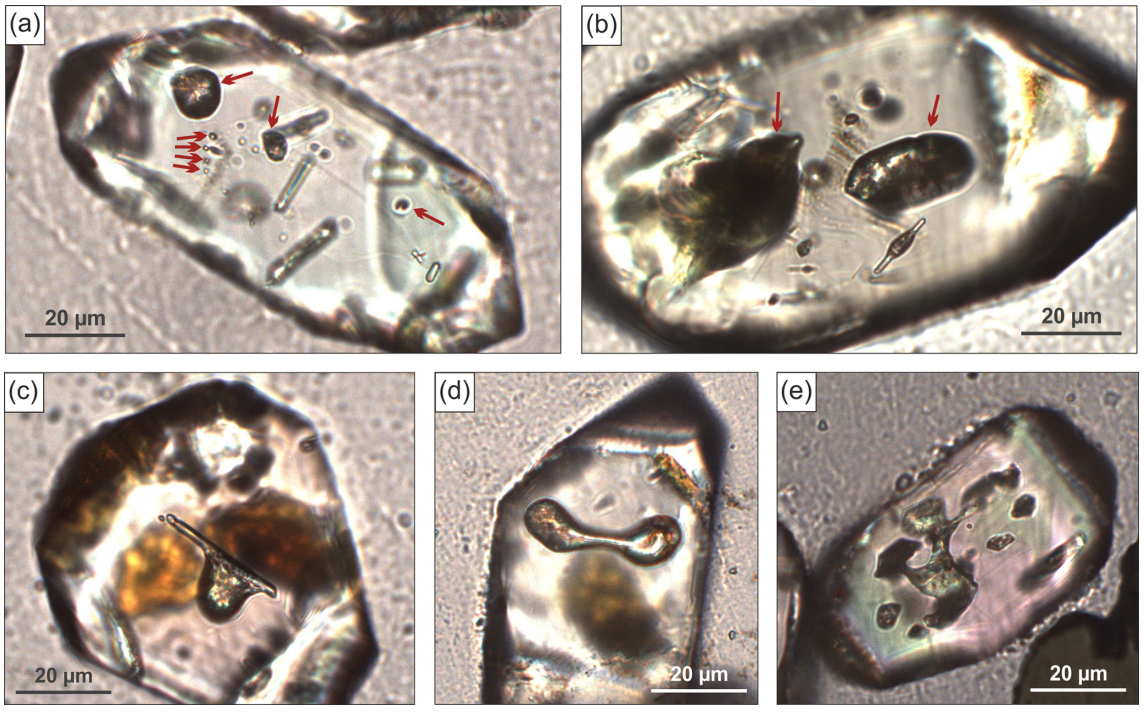


**Figure 5.** Typical morphology of MIs in zircon from acid SBRF rocks: **(a)** dark subhedral bubbles (marked with red arrows) and apatite needles, **(b)** multiphase MIs (marked with red arrows), **(c)** MI attached to an apatite needle, **(d)** anhedral wormlike MI, and **(e)** anhedral amoeboidlike MI.

Kanzaki et al. (2012) and Romanenko et al. (2021) repeated a similar experiment, where kokchetavite was obtained by dehydrating K-cymrite at ambient pressure and heating it up to 750 °C. The first record of a natural kokchetavite, found as a micrometre-size inclusion within MSI in clinopyroxene and garnet in a garnet–pyroxene rock from the Kokchetav UHP terrane (Hwang et al., 2004, 2013), was interpreted as non-equilibrium precipitation during exhumation, i.e. as being due to the fluid/melt infiltration. Working on the same complex, Mikhno et al. (2013) suggested that kokchetavite formed through the dehydration of K-cymrite, but the exact $P$–$T$ conditions for such a transition were not determined.

Kumdykolite and kokchetavite, along with coesite and diamond, have been regarded for some time by the petrological community as being indicators of UHP metamorphism (Hwang et al., 2009, 2013; Kotková et al., 2014; Romanenko et al., 2021). More findings of kumdykolite and/or kokchetavite have been reported recently, such as multiphase inclusions with kokchetavite in detrital garnet from UHP metamorphic terrane in eastern Papua New Guinea (Baldwin et al., 2021) and kumdykolite and kokchetavite in multiphase inclusions (together with cristobalite) in garnets from UHP terrains in the central Saxonian Erzgebirge in the northwestern Bohemian Massif in Germany (Schönig et al., 2020). Stähle et al. (2022) reported the finding of kokchetavite, together with some other UHP phases, in alkali-rich melt glass (shock-induced melt veins) in weakly to moderately shocked amphibolite clasts from the young Ries impact crater in southern Germany (age of structure: 14.8 Ma). Here kokchetavite is found to be in an association with other UHP minerals (liebermannite, albitic jadeite and the immediate vicinity of majoritic garnet), which may indicate crystallisation pressures of nearly 10 GPa.

However, Ferrero et al. (2016) suggested that the presence of kumdykolite and kokchetavite does not necessarily represent UHP conditions. In their research, kumdykolite and kokchetavite were found together with cristobalite, mica and calcite in high-pressure granulites of the Orlica–Śnieżnik Dome (Bohemian Massif). As the maximum pressure recorded in these host rocks by the entrapment conditions of MI is 2.7 GPa (with an entrapment temperature of 875 °C, which is below the quartz–coesite transition; Ferrero et al., 2015), their observations indicate that (ultra)-high pressure is not required for the formation of kumdykolite and kokchetavite. Instead, together with cristobalite, these polymorphs are the product of partial melt crystallisation in preserved nanogranites, i.e. MSI interpreted as former MI. Furthermore, Ferrero and Angel (2018) also reported nanogranites with kumdykolite and kokchetavite in low-pressure garnet xenocrysts of the La Galite archipelago in Tunisia, trapped at 0.4–0.5 GPa (Ferrero et al., 2014). Our study, in which kumdykolite and kokchetavite were found in multiphase MI in magmatic zircon from the acid rocks of the SBRF, further corroborates that such phases cannot be used

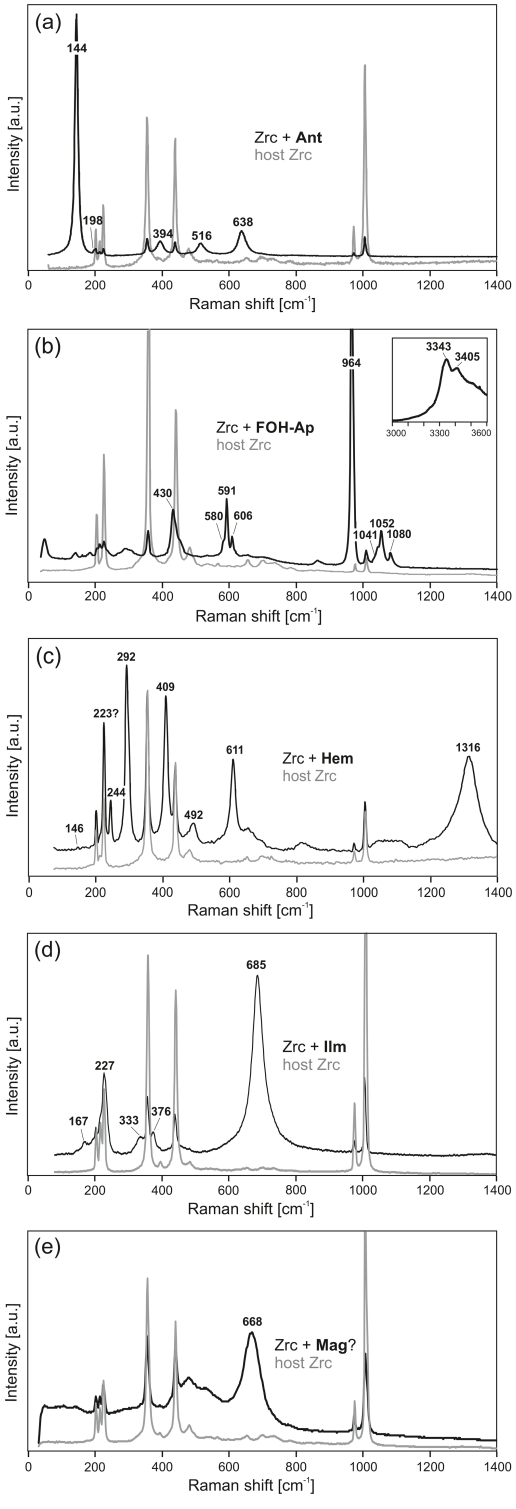


**Figure 6.** Typical Raman spectra of the mineral inclusions detected in zircon from acid SBRF rocks, with spectra of host zircon in grey for comparison (Zrc): **(a)** anatase; **(b)** apatite with a spectrum characteristic of fluor- to hydroxyfluorapatite (FOH), after Penel et al. (1997); **(c)** hematite; **(d)** ilmenite; and **(e)** magnetite with only the strongest band at 668 $cm^{-1}$ present. Only bands that belong to the inclusions are labelled. Abbreviations are defined in Table 1.

as evidence for UHP (or even HP) conditions because their formation here appears to be completely independent of pressure.

### 5.2 Anatase

Anatase is found here as a single mineral inclusion in zircon from acid igneous rocks. It is one of three naturally occurring $TiO_2$ polymorphs, the other two being rutile and brookite. It is generally considered to form, similar to brookite, in low-temperature hydrothermal environments (Lindsley, 1991). Among those three $TiO_2$ polymorphs, rutile is the most common phase in nature and is thought to be the only polymorph with a true stability field, whereas anatase and brookite are regarded as metastable. Rutile is also denser than anatase (4.2 g $cm^{-3}$ compared to 3.8 g $cm^{-3}$, Wenk and Bulakh, 2004) and is therefore considered stable at both higher temperatures and pressures compared to anatase. However, all the published "phase boundaries" between rutile and anatase or brookite most probably reflect kinetics rather than equilibrium (Lindsley, 1991).

Experimental studies in the field of materials science (e.g. Gopal et al., 1997; Li and Ishigaki, 2002; Smith et al., 2009; Hanaor and Sorrell, 2011; Fu et al., 2013) have shown that the rate of crystallisation from solution is what actually determines which $TiO_2$ phase is stabilised. Li and Ishigaki (2002) showed that the nucleation of anatase and rutile from melt depends on the degree of undercooling of the melt or the solidification temperature, with anatase being favoured under a high cooling rate and rutile under near-equilibrium solidification conditions. More rapid crystallisation of metastable anatase could be explained with the lower surface energy of this polymorph, despite the lower Gibbs free energy of thermodynamically stable rutile (Li and Ishigaki, 2002; Hanaor and Sorrell, 2010). Although anatase and brookite are found to transform irreversibly to rutile at different temperatures (Fu et al., 2013), anatase captured in mechanically resistant zircon is protected from any further phase transformations and may possibly be regarded as an indicator of a high cooling rate in our magmatic system.

### 5.3 Iron oxides

Various iron oxides were detected as inclusions in magmatic zircon from SBRF, either as individual mineral inclusions (ilmenite, hematite and possibly magnetite) or within the MI (hematite). In igneous rocks ilmenite has been reported to have exsolution lamellae, decomposing into hematite and anatase (Haggerty, 1991). In the case of acid SBRF rocks, where the inclusions are sealed within zircon and protected from later re-equilibration and changes in the crystal lattice, such a scenario is unlikely. Magnetite, and especially hematite, as minerals with ferric iron, suggests initially (very-)high-oxygen fugacities. Although ilmenite contains ferrous iron, it was detected (only in the TRES sample)

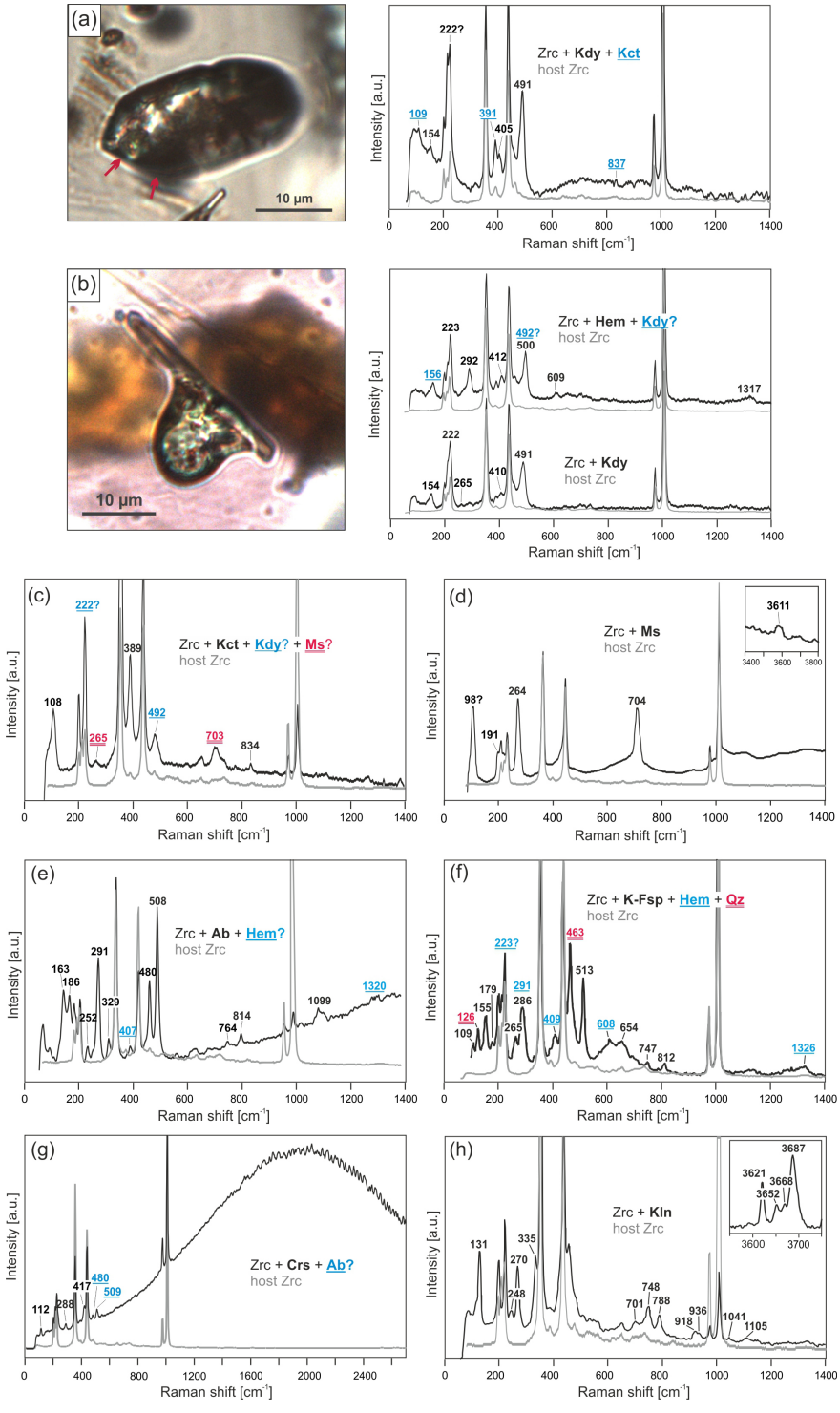


**Figure 7.** Raman spectra of MI revealing various silicates and polymorph phases, with spectra of host zircon in grey for comparison (Zrc): **(a)** MI enlarged from Fig. 5b with smaller (daughter) crystals visible in the lower-left corner of the MI. Detected phases include kumdykolite and kokchetavite. **(b)** MI attached to apatite, enlarged from Fig. 5c, containing hematite (very fine red dots in the MI) and kumdykolite. **(c)** Raman spectrum from the MI of kokchetavite and possible kumdykolite and muscovite. **(d)** Raman spectrum of muscovite detected in MI. **(e)** Raman spectrum from the MI in Fig. 5d of albite and possibly hematite. **(f)** Raman spectrum from MI, K-feldspar, hematite and quartz. **(g)** Raman spectrum from the MI in Fig. 5e, cristobalite with a characteristic "hump" in the higher wavenumbers and albite. **(h)** Raman spectrum from the MI in Fig. 5d with kaolinite. Only bands that belong to the inclusions are labelled. Abbreviations are defined in Table 1.

in association with hematite and possible magnetite inclusions. Therefore, the iron oxides detected in magmatic zircon, where they represent primary inclusions, are here evidence of oxidised early conditions of melt crystallisation.

### 5.4 Apatite

The most mineral inclusions in zircon are by far apatite, recognisable by an elongated, needlelike habitus. Apatite inclusions are common in zircon (Jennings et al., 2011), and, as stated in Schneider et al. (2022), in the case of SBRF, apatite crystallised prior to or during the crystallisation of zircon. Apatite inclusions in zircon have a high potential for constraining the early magma composition and for tracking the behaviour and content of volatiles in magmatic systems, where F or Cl contents in apatite can be used to delineate petrogenetic processes (Kendall-Langley et al., 2021). This is especially used in the detrital zircon study, as apatite compositions match those of apatite in the host rock matrix (Jennings et al., 2011). As the composition of the acid rocks of SBRF and apatite is already known (Schneider et al., 2022), providing a detailed chemical composition of apatite was not the focus of this study. Nevertheless, it is worth pointing out that most of the apatite Raman spectra resemble fluorapatite, with only a minor concentration of "water" (OH), consistent with crystallisation from relatively dry magma as stated in Balen et al. (2020) and Schneider et al. (2022). According to Piccoli and Candela (2002), fluorapatite is by far the most common member of the apatite family found in igneous rocks.

### 5.5 Implications for magmatic evolution

As pointed out in Balen et al. (2020) and Schneider et al. (2022), zircon from acid rocks of SBRF represents early-crystallised zircon. Therefore, the inclusions studied here likely record the early history of melt crystallisation and magmatic conditions, especially as they are clearly isolated systems protected from the later re-equilibration by the absence of cracks connecting the inclusion to the rock matrix. Inclusions of anatase indicate rapid cooling, while the iron oxides indicate oxidised conditions. However, the most exciting and important findings here are MIs with kumdykolite and kokchetavite.

The inclusions in zircon have been studied more intensively in the last few decades but mostly from metamorphic rocks, where it served as a capsule for reconstructing metamorphic history (e.g. Liu et al., 2001; Rubatto and Hermann, 2007; Katayama and Maruyama, 2009; Liu and Liou, 2011; Perraki and Faryad, 2014; Zhang et al., 2017; Gonzalez et al., 2021; Fei and Liu, 2022), and less frequently in igneous petrology (e.g. Jennings et al., 2011; Gudelius et al., 2020; Zeng et al., 2020). To the best of our knowledge, crystallised MIs containing kumdykolite and kokchetavite in magmatic zircon have not been reported yet. The very few documented findings of these polymorphs in zircon relate to UHP terrains (Perraki and Faryad, 2014; Fei and Liu, 2022). To be preserved, such metastable mineral inclusions should remain as isolated systems, trapped within mechanically strong host minerals, such as garnet or zircon (Ferrero and Angel, 2018). Our study with micro-Raman spectroscopy is the first of its kind on MI from magmatic zircon, although not the first study of MI in zircon from igneous rocks in general. Gudelius et al. (2020) studied the mineralogical and chemical compositions of MI in mafic and felsic rocks of the Bushveld Complex (South Africa) using EPMA, which cannot determine the exact polymorph. Furthermore, they performed rehomogenisation and re-crystallisation of the MI, a procedure in which the original metastable polymorphs (if present) are lost because they are remelted completely. As a result, we here report the first finding of these polymorph minerals in magmatic zircon from acid rocks, both intrusive and effusive.

Formation of kokchetavite through dewatering of K-cymrite is highly unlikely in the case of acid SBRF igneous rocks, as K-cymrite is a UHP mineral (Massonne, 1995). Kumdykolite and kokchetavite are interpreted as crystallisation products of the melt trapped as the inclusion and are the result of rapid crystallisation of a melt (Ferrero and Angel, 2018). As suggested in Ferrero and Angel (2018), when the melt is trapped in a small pore in metamorphic rocks, rapid crystallisation is not caused by rapid cooling but rather by the peculiar undercooled and supersaturated conditions achieved during cooling by a melt confined in a small cavity. However, the acid SBRF igneous rocks are the result of the crystallisation of deep-seated magmas which were rapidly transported toward the surface along the extensional deep faults, a process which consequently caused rapid cooling (Belak et al., 1998; Balen et al., 2020; Schneider et al., 2022). The occurrence of anatase inclusions as a primary $TiO_2$ phase in zircon is independent evidence of such a scenario. Therefore, the formation of these polymorphs in zircon from acid rocks, in addition to undercooling and supersaturation conditions, was likely also favoured by rapid cooling due to rapid exhumation.

## 6 Conclusions

Mineral inclusions found in magmatic zircon from granite and rhyolites of SBRF comprise anatase, apatite, hematite, ilmenite and potentially magnetite, while MIs contain various polymorphs of feldspars (albite, K-feldspar, kokchetavite and kumdykolite), $SiO_2$ (quartz or cristobalite), hematite and phyllosilicates (kaolinite and muscovite). MIs with such composition represent nanogranitoids. Compared to the nanogranitoids of anatectic origin previously reported in partially melted rocks, here they represent primary inclusions of parental magma (i.e. magmatic nanogranitoids) that were protected from later equilibration with the melt or alteration by fluids. In this study we report for the first time

kumdykolite- and kokchetavite-bearing MI in magmatic zircon. The presence of kumdykolite and kokchetavite in the MI hosted in magmatic zircon is possibly the strongest evidence that these phases should not be considered exclusively UHP (nor even HP) phases.

Inclusions found here are independent mineralogical evidence indicating rapid uplift and emplacement of a primarily oxidised magma from the deep (lower) crustal level. The rapid uplift was possible due to the formation of extensional deep faults during the tectonic transition from compression to extension in the Late Cretaceous ($\sim$ 82 Ma) and the regional geological event associated with the closure of the Neotethys Ocean in the area of present-day Slavonian mountains.

*Data availability.* Data are available upon contacting the corresponding author.

*Author contributions.* PS designed the research on inclusions, carried out detailed measurements, analysed the data, wrote the paper and prepared the visualisation; DB collected the samples, designed the research, and contributed to the preparation and editing of the paper.

*Competing interests.* The contact author has declared that neither of the authors has any competing interests.

*Disclaimer.* Publisher's note: Copernicus Publications remains neutral with regard to jurisdictional claims made in the text, published maps, institutional affiliations, or any other geographical representation in this paper. While Copernicus Publications makes every effort to include appropriate place names, the final responsibility lies with the authors.

*Special issue statement.* This article is part of the special issue "Probing the Earth: Melt and solid inclusions as probes to understand nature". It is not associated with a conference.

*Acknowledgements.* The authors are grateful to Jarmila Luptáková (†) from the Earth Science Institute in Banská Bystrica for her help with Raman spectroscopy. Our gratitude goes to Marián Putiš from Comenius University in Bratislava, our host in Slovakia, and to Christoph Hauzenberger and Etienne Skrzypek from the Department of Earth Sciences (Petrology and Geochemistry) at the University of Graz for their supervision and help. The work of Silvio Ferrero and the anonymous reviewer in improving the paper is greatly appreciated.

*Financial support.* The Go Styria scholarship programme was supported by funding from the province of Styria for research at the Department of Earth Sciences (Petrology and Geochemistry) at the University of Graz. The CEEPUS exchange programme (grant nos. RO-0038-14-1819 and RO-0038-13-1718) supported research at the Earth Science Institute in Banská Bystrica. Sampling campaigns and fieldwork were carried out and financially supported within the framework of an HRZZ (Croatian Science Foundation) project (grant no. IP-2014-09-9541).

*Review statement.* This paper was edited by Matteo Alvaro and reviewed by Silvio Ferrero and one anonymous referee.

## References

Audétat, A. and Lowenstern, J. B.: Melt Inclusions, in: Treatise on Geochemistry, Second Edition, edited by: Holland, H. D. and Turekian, K. K., Elsevier, Oxford, 13, 143–173, https://doi.org/10.1016/B978-0-08-095975-7.01106-2, 2014.

Baldwin, S. L., Schönig, J., Gonzalez, J. P., Davies, H., and von Eynatten, H.: Garnet sand reveals rock recycling processes in the youngest exhumed high- and ultrahigh-pressure terrane on Earth, P. Natl. Acad. Sci. USA, 118, e2017231118, https://doi.org/10.1073/pnas.2017231118, 2021.

Balen, D. and Petrinec, Z.: Development of columnar jointing in albite rhyolite in a rapidly cooling volcanic environment (Rupnica, Papuk Geopark, Croatia), Terra Nova, 26, 102–110, https://doi.org/10.1111/ter.12075, 2014.

Balen, D., Schneider, P., Massonne, H.-J., Opitz, J., Luptakova, J., Putiš, M., and Petrinec, Z.: The Late Cretaceous A-type alkali-feldspar granite from Mt. Požeška Gora (N Croatia): Potential marker of fast magma ascent in the Europe–Adria suture zone, Geol. Charpath., 71, 361–381, https://doi.org/10.31577/GeolCarp.71.4.5, 2020.

Balen, D., Schneider, P., Petrinec, Z., Radonić, G., and Pavić, G.: Cretaceous Volcanic Rock Geosites of the Papuk UNESCO Global Geopark (Croatia): Scientific Aspect of Geoheritage in Geoeducation, Geotourism and Geoconservation, Geoconserv. Res., 6, 1–17, https://doi.org/10.30486/gcr.2023.1979814.1122, 2023.

Bartoli, O. and Cesare, B.: Nanorocks: a 10-year-old story, Rend. Fis. Acc. Lincei, 31, 249–257, https://doi.org/10.1007/s12210-020-00898-7, 2020.

Belak, M., Halamić, J., Marchig, V., and Tibljaš, D.: Upper Cretaceous-Palaeogene Tholeiitic Basalts of the Southern Margin of the Pannonian Basin: Požeska gora Mt. (Croatia), Geol. Croat., 51, 163–174, https://doi.org/10.4154/GC.1998.13, 1998.

Bodnar, R. J. and Student, J. J.: Melt inclusions in plutonic rocks: Petrography and microthermometry. In: Melt Inclusions in Plutonic Rocks, Mineralogical Association of Canada Short Course Series, edited by: Webster, J. D., Mineralogical Association of Canada, Montreal, 36, 1–25, 2006.

Cesare, B., Ferrero, S., Salvioli-Mariani, E., Pedron, D., and Cavallo, A.: Nanogranite and glassy inclusions: the anatectic melt in migmatites and granulites, Geology, 37, 627–630, https://doi.org/10.1130/G25759A.1, 2009.

Cesare, B., Acosta-Vigil, A., Ferrero, S., Bartoli, O.: Melt Inclusions in Migmatites and Granulites, in: The Science of Microstructure – Part II, edited by: Forster, M. A. and Fitz Gerald,

J. D., Electronic edition, Journal of the Virtual Explorer, 38, 2, https://doi.org/10.3809/jvirtex.2011.00268, 2011.

Cesare, B., Acosta-Vigil, A., Bartoli, O., and Ferrero, S.: What can we learn from melt inclusions in migmatites and granulites?, Lithos, 239, 186–216, https://doi.org/10.1016/j.lithos.2015.09.028, 2015.

Fei, C. and Liu, J.: Vaterite in a decrepitated diamond-bearing inclusion in zircon from a stromatic migmatite in the Chinese Sulu ultrahigh-pressure metamorphic belt, Am. Mineral., 107, 1410–1424, https://doi.org/10.2138/am-2021-7940, 2022.

Ferrero, S. and Angel, R. J.: Micropetrology: Are Inclusions Grains of Truth?, J. Petrol., 59, 1671–1700, https://doi.org/10.1093/petrology/egy075, 2018.

Ferrero, S., Bartoli, O., Cesare, B., Salvioli-Mariani, E., Acosta-Vigil, A., Cavallo, A., Groppo, C., and Battiston, S.: Microstructures of melt inclusions in anatectic metasedimentary rocks, J. Metamorph. Geol., 30, 303–322, https://doi.org/10.1111/j.1525-1314.2011.00968.x, 2012.

Ferrero, S., Braga, R., Berkesi, M., Cesare, B., and Laridhi Ouazaa, N.: Production of metaluminous melt during fluid-present anatexis: an example from the Maghrebian basement, La Galite Archipelago, central Mediterranean, J. Metamorph. Geol., 32, 209–225, https://doi.org/10.1111/jmg.12068, 2014.

Ferrero, S., Wunder, B., Walczak, K., O'Brien, P. J., and Ziemann, M. A.: Preserved near ultrahigh-pressure melt from continental crust subducted to mantle depths, Geology, 43, 447–450, https://doi.org/10.1130/G36534.1, 2015.

Ferrero, S., Ziemann, M. A., Angel, R. J., O'Brien, P. J., and Wunder, B.: Kumdykolite, kokchetavite, and cristobalite crystallized in nanogranites from felsic granulites, Orlica–Snieznik Dome (Bohemian Massif): not evidence for ultrahigh–pressure conditions, Contrib. Mineral. Petrol., 171, 3, https://doi.org/10.1007/s00410-015-1220-x, 2016

Frezzotti, M. L.: Silicate-melt inclusions in magmatic rocks: Applications to petrology, Lithos, 55, 273–299, https://doi.org/10.1016/S0024-4937(00)00048-7, 2001.

Frezzotti, M. L., Tecce, F., and Casgali, A.: Raman spectroscopy for fluid inclusions analysis, J. Geochem. Explor., 112, 1–12, https://doi.org/10.1016/j.gexplo.2011.09.009, 2012.

Fu, Z., Liang, Y., Wang, S., and Zhong, Z.: Structural phase transition and mechanical properties of $TiO_2$ under high pressure, Phys. Status Solidi B, 250, 2206–2214, https://doi.org/10.1002/pssb.201349186, 2013.

Gonzalez, J. P., Mazzucchelli, M. L., Angel, R. J., and Alvaro, M.: Elastic Geobarometry for Anisotropic Inclusions in Anisotropic Host Minerals: Quartz-in-Zircon, J. Geophys. Res.-Sol. Ea., 126, 6, e2021JB022080, https://doi.org/10.1029/2021JB022080, 2021.

Gopal, M., Moberly Chan, W. J., and De Jonghe, L. C.: Room temperature synthesis of crystalline metal oxides, J. Mater. Sci., 32, 6001–6008, https://doi.org/10.1023/A:1018671212890, 1997.

Gudelius, D., Zeh, A., Almeev, R. R., Wilson, A. H., Fischer, L. A., and Schmitt, A. K.: Zircon melt inclusions in mafic and felsic rocks of the Bushveld Complex – Constraints for zircon crystallization temperatures and partition coefficients, Geochim. Cosmochim. Ac., 289, 158–181, https://doi.org/10.1016/j.gca.2020.08.027, 2020.

Haggerty, S. E.: Oxide textures – a mini-atlas, Rev. Mineral. Geochem., 25, 129–220, https://doi.org/10.1515/9781501508684-008, 1991.

Hanaor, D. A. H. and Sorrell, C. C.: Review of the anatase to rutile phase transformation, J. Mat. Sci., 46, 855–874, https://doi.org/10.1007/s10853-010-5113-0, 2011.

Harley, S. L. and Kelly, N. M.: Zircon Tiny but Timely, Elements, 3, 13–18, https://doi.org/10.2113/gselements.3.1.13, 2007.

Horvat, M.: Geochemistry and petrology of granitoids of Papuk and Psunj Mts. (Slavonia, Croatia), PhD Thesis, Eötvös Loránd University, Budapest, Hungary, 133 pp., 2004.

Hoskin, P. W. O. and Schaltegger, U.: The composition of zircon and igneous and metamorphic petrogenesis, Rev. Mineral. Geochem., 53, 27–62, https://doi.org/10.2113/0530027, 2003.

Hwang, S.-L., Shen, P., Chu, H.-T., Tzen, Y. T., Liou, J. G., Sobolev, N. V., Zhang, R.-Y., Shatsky, V. S., and Zayachkovsky, A. A.: Kokchetavite: A new potassium-feldspar polymorph from the Kokchetav ultrahigh-pressure terrane, Contrib. Mineral. Petrol., 148, 380–389, https://doi.org/10.1007/s00410-004-0610-2, 2004.

Hwang, S.-L., Shen, P., Chu, H.-T., Yui, T.-F., Liou, J. G., and Sobolev, N. V.: Kumdykolite, an orthorhombic polymorph of albite, from the Kokchetav ultrahigh-pressure massif, Kazakhstan, Eur. J. Mineral., 21, 1325–1334, https://doi.org/10.1127/0935-1221/2009/0021-1970, 2009.

Hwang, S.-L., Yui, T.-F., Chu, H.-T., Shen, P., Liou, J. G, and Sobolev N. V.: Oriented kokchetavite compound rods in clinopyroxene of Kokchetav ultrahigh-pressure rocks, J. Asian Earth Sci., 63, 56–69, https://doi.org/10.1016/j.jseaes.2012.09.003, 2013.

Jamičić, D.: Osnovne geološke značajke Slavonskih planina s osvrtom na Našičko područje, Matica Hrvatska, Našički zbornik, 6, 29–36, 2001 (in Croatian).

Jamičić, D.: Osnovne geološke značajke Slavonskih planina, Priroda, 6–7, 20–27, 2003 (in Croatian).

Jennings, E., Marschall, H., Hawkesworth, C., and Storey, C.: Characterization of magma from inclusions in zircon: Apatite and biotite work well, feldspar less so, Geology, 39, 863–866, https://doi.org/10.1130/G32037.1, 2011.

Kanzaki M., Xue X., Amalberti J., and Zhang Q.: Raman and NMR spectroscopic characterization of high-pressure K-cymrite ($KAlSi_3O_8 \cdot H_2O$) and its anhydrous form (kokchetavite), J. Mineral. Petrol. Sci., 107, 114–119, https://doi.org/10.2465/jmps.111020i, 2012.

Katayama, I. and Maruyama, S.: Inclusion study in zircon from ultrahigh-pressure metamorphic rocks in the Kokchetav massif: An excellent tracer of metamorphic history, J. Geol. Soc., 166, 783–796, https://doi.org/10.1144/0016-76492008-019, 2009.

Kendall-Langley, L. A., Kemp, A. I. S., Hawkesworth, C. J., EIMF, Roberts, M. P.: Quantifying F and Cl concentrations in granitic melts from apatite inclusions in zircon, Contrib. Mineral. Petrol., 176, 58, https://doi.org/10.1007/s00410-021-01813-5, 2021.

Kloprogge, T.: Raman Spectroscopy of Clay Minerals, in: Developments in Clay Science, 8, edited by: Gates, W. P., Kloprogge, J. T., Madejová, J., and Bergaya, F., Elsevier, 150–199, https://doi.org/10.1016/B978-0-08-100355-8.00006-0, 2017.

Kotková J., Škoda R., and Machovič, V.: Kumdykolite from the ultrahigh-pressure granulite of the Bohemian Massif, Am.

Mineral., 99, 1798–1801, https://doi.org/10.2138/am.2014.4889, 2014.

Li, Y. and Ishigaki, T.: Thermodynamic Analysis of Nucleation of Anatase and Rutile from $TiO_2$ Melt, J. Cryst. Growth., 242, 511–516, https://doi.org/10.1016/S0022-0248(02)01438-0, 2002.

Lindsley, D. H.: Experimental studies of oxide minerals, Rev. Mineral. Geochem., 25, 69–106, https://doi.org/10.1515/9781501508684-006, 1991.

Liu, F. L. and Liou, J. G.: Zircon as the best mineral for P–T–time history of UHP metamorphism: A review on mineral inclusions and U–Pb SHRIMP ages of zircons from the Dabie–Sulu UHP rocks, J. Asian Earth Sci., 40, 1–39, https://doi.org/10.1016/j.jseaes.2010.08.007, 2011.

Liu, J., Ye, K., Maruyama, S., Cong, B., and Fan, H.: Mineral Inclusions in Zircon from Gneisses in the Ultrahigh-Pressure Zone of the Dabie Mountains, China, J. Geol., 109, 523–535, https://doi.org/10.1086/320796, 2001.

Lowenstern, J. B.: Melt inclusions come of age: Volatiles, volcanoes and Sorby's legacy, in: Developments in Volcanology, Melt Inclusions in Volcanic Systems, edited by: De Vivo, B. and Bodnar, R. J., Elsevier, Amsterdam, 5, 1–21, https://doi.org/10.1016/S1871-644X(03)80021-9, 2003.

Lužar-Oberiter, B., Mikes, T., Dunkl, I., Babić, Lj., and Von Eynatten, H.: Provenance of Cretaceous synorogenic sediments from the NW Dinarides (Croatia), Swiss J. Geosci., 105, 377–399, https://doi.org/10.1007/s00015-012-0107-3, 2012.

Massonne, H.-J.: Experimental and petrogenetic study of UHPM, in "Ultrahigh Pressure Metamorphism", edited by: Coleman, R. G. and Wang, X., Cambridge University Press, New York, 33–95, https://doi.org/10.1017/CBO9780511573088.003, 1995.

Mikhno, A. O., Schmidt, U., and V. Korsakov, A. V.: Origin of K-cymrite and kokchetavite in the polyphase mineral inclusions from Kokchetav UHP calc-silicate rocks: evidence from confocal Raman imaging, Eur. J. Mineral., 25, 807–816, https://doi.org/10.1127/0935-1221/2013/0025-2321, 2013.

Nèmeth, P., Lehner, S., Petaev, M., and Buseck, P.: Kumdykolite, a high-temperature feldspar from an enstatite chondrite, Am. Mineral., 98, 1070–1073, https://doi.org/10.2138/am.2013.4459, 2013.

Nicoli, G. and Ferrero, S.: Nanorocks, volatiles and plate tectonics, Geosci. Front., 12, 101188, https://doi.org/10.1016/j.gsf.2021.101188, 2021.

Pamić, J.: Upper Cretaceous basaltoid and pyroclastic rocks from the Voćin volcanic mass on the Papuk Mt. (Slavonija, Northern Croatia), Geol. Vjesnik, 44, 161–172, 1991 (in Croatian, with English summary).

Pamić, J.: Eoalpine to Neoalpine magmatic and metamorphic processes in the northwestern Vardar Zone, the easternmost Periadriatic Zone and the southwestern Pannonian Basin, Tectonophysics, 109, 273–307, https://doi.org/10.1016/0040-1951(93)90135-7, 1993.

Pamić, J.: Volcanic rocks of the Sava-Drava interfluve and Baranja (Croatia), Nafta, Zagreb, Croatia, 192 pp., ISBN 953-96835-1-3, 1997 (in Croatian, with English summary).

Pamić, J.: The Sava-Vardar Zone of the Dinarides and Hellenides versus the Vardar Ocean, Eclogae Geol. Helv., 95, 99–113, https://doi.org/10.5169/seals-168948, 2002.

Pamić, J. and Lanphere, M.: Hercynian granites and metamorphic rocks from the Papuk, Psunj, Krndija and the surrounding basement of the Pannonian Basin (Northern Croatia, Yugoslavia), Geologija Ljubljana, 34, 81–253, https://doi.org/10.5474/geologija.1991.004, 1991a.

Pamić, J. and Lanphere, M.: A-type granites from the collisional area of the northernmost Dinarides and Pannonian Basin, Neues Jahrb. Mineral. Abh., 161, 215–236, 1991b.

Pamić, J., Belak, M., Bullen, T. D., Lanphere, M. A., and McKee, E. H.: Geochemistry and geodynamics of a Late Cretaceous bimodal volcanic association from the southern part of the Pannonian Basin in Slavonija (northern Croatia), Mineral. Petrol., 68, 271–296, https://doi.org/10.1007/s007100050013, 2000.

Pamić, J., Tomljenović, B., and Balen, D.: Geodynamic and petrogenetic evolution of Alpine ophiolites from the central and NW Dinarides: an overview, Lithos, 65, 113–142, https://doi.org/10.1016/S0024-4937(02)00162-7, 2002a.

Pamić, J., Balen, D., and Herak, M.: Origin and geodynamic evolution of Late Paleogene magmatic associations along the Periadriatic-Sava-Vardar magmatic belt, Geodin. Acta, 15, 209–231, https://doi.org/10.1016/S0985-3111(02)01089-6, 2002b.

Penel, G., Leroy, G., Rey, C., Sombret, B., Huvenne, J., and Brès, E. F.: Infrared and Raman microspectrometry study of fluor-fluor-hydroxy and hydroxy-apatite powders, J. Mater. Sci., 8, 271–276, https://doi.org/10.1023/A:1018504126866, 1997.

Perraki, M. and Faryad, S. W.: First finding of microdiamond, coesite and other UHP phases in felsic granulites in the Moldanubian Zone: Implications for deep subduction and a revised geodynamic model for Variscan Orogeny in the Bohemian Massif, Lithos, 202, 157–166, https://doi.org/10.1016/j.lithos.2014.05.025, 2014.

Piccoli, P. M. and Candela, P. A.: Apatite in Igneous Systems, Rev. Mineral. Geochem., 48, 255–292, https://doi.org/10.2138/rmg.2002.48.6, 2002.

Romanenko, A., Rashchenko, S., Sokol, A., Korsakov, A., Seryotkin, Y., Glazyrin, K., and Musiyachenko, K.: Crystal structures of K-cymrite and kokchetavite from single-crystal X-ray diffraction, Am. Mineral., 106, 404–409, https://doi.org/10.2138/am-2020-7407, 2021.

RRUFF: Albite R040068, https://rruff.info/albite/display=default/R040068, last access: 1 September 2023a.

RRUFF: Cristobalite R060648, https://rruff.info/cristobalite/R060648, last access: 1 September 2023b.

RRUFF: Hematite R040024, https://rruff.info/hematite/R040024, last access: 1 September 2023c.

RRUFF: Ilmenite R130214, https://rruff.info/ilmenite/R130214, last access: 1 September 2023d.

RRUFF: Microcline R040154, https://rruff.info/microcline/R040154, last access: 1 September 2023e.

RRUFF: Quartz R050125, https://rruff.info/quartz/R050125, last access: 1 September 2023f.

Rubatto, D. and Hermann, J.: Zircon Behaviour in Deeply Subducted Rocks, Elements, 3, 31–35, https://doi.org/10.2113/gselements.3.1.31, 2007.

Schmid, S. M., Bernoulli, D., Fügenschuh, B., Matenco, L., Schefer, S., Schuster, R., Tischler, M., and Ustaszewski, K.: The Alps–Carpathians–Dinarides connection: a compilation of tectonic units, Swiss J. Geosci., 101, 139–183, https://doi.org/10.1007/s00015-008-1247-3, 2008.

Schmid, S. M., Fügenschuh, B., Kounov, A., Maţenco, L., Nievergelt, P., Oberhänsli, R., Pleuger, J., Schefer, S., Schuster, R.,

Tomljenović, B., Ustaszewski, K., and Van Hinsbergen, D. J. J.: Tectonic units of the Alpine collision zone between Eastern Alps and western Turkey, Gondwana Res., 78, 308–374, https://doi.org/10.1016/j.gr.2019.07.005, 2020.

Schneider, P., Balen, D., Opitz, J., and Massonne, H.-J.: Dating and geochemistry of zircon and apatite from rhyolite at the UNESCO geosite Rupnica (Mt. Papuk, northern Croatia) and the relationship to the Sava Zone, Geol. Croat., 75, 249–267, https://doi.org/10.4154/gc.2022.19, 2022.

Schönig, J., von Eynatten, H., Meinhold, G., Lünsdorf, N. K., Willner, A. P., and Schulz, B.: Deep subduction of felsic rocks hosting UHP lenses in the central Saxonian Erzgebirge: Implications for UHP terrane exhumation, Gondwana Res., 87, 320–329, https://doi.org/10.1016/j.gr.2020.06.020, 2020.

Seki, Y. and Kennedy, G. C.: The breakdown of potassium feldspar, $KAlSi_3O_8$, at high temperatures and high pressures, Am. Mineral., 49, 1688–1706, 1964.

Smith, S., Stevens, R., Liu, S., Li, G., Navrotsky, A., Boerio-Goates, J., and Woodfield, B.: Heat capacities and thermodynamic functions of $TiO_2$ anatase and rutile: Analysis of phase stability, Am. Mineral., 94, 236–243, https://doi.org/10.2138/am.2009.3050, 2009.

Sorby, H. C.: On the microscopical structure of crystals, indicating origin of minerals and rocks, Quart. J. Geol. Soc. London, 14, 453–500, https://doi.org/10.1144/GSL.JGS.1858.014.01-02.44, 1858.

Stähle, V., Chanmuang, N. C., Schwarz, W. H., Trieloff, M., and Varychev, A.: Newly detected shock-induced high-pressure phases formed in amphibolite clasts of the suevite breccia (Ries impact crater, Germany): Liebermannite, kokchetavite, and other ultrahigh-pressure phases, Contrib. Mineral, Petrol., 177, 80, https://doi.org/10.1007/s00410-022-01936-3, 2022.

Thomas, J. B., Bodnar, R. J., Shimizu, N., and Sinha, A. K.: Determination of zircon/melt trace element partition coefficients from SIMS analysis of melt inclusions in zircon, Geochim. Cosmochim. Ac., 66, 2887–2902, https://doi.org/10.1016/S0016-7037(02)00881-5, 2002.

Thomas, J., Bodnar, R., Shimizu, N., and Chesner, C.: Melt Inclusions in Zircon, Rev. Mineral. Geochem., 53, 63–87, https://doi.org/10.2113/0530063, 2003.

Thompson, P., Parsons, I., Graham, C. M., and Jackson, B.: The breakdown of potassium feldspar at high water pressures, Contrib. Mineral. Petrol., 130, 176–186, https://doi.org/10.1007/s004100050358, 1998.

Ustaszewski, K., Schmid, S. M., Lugović, B., Schuster, R., Schaltegger, U., Bernoulli, D., Hottinger, L., Kounov, A., Fügenschuh, B., and Schefer, S.: Late Cretaceous intra-oceanic magmatism in the internal Dinarides (northern Bosnia and Herzegovina): implications for the collision of the Adriatic and European plates, Lithos, 108, 106–125, https://doi.org/10.1016/j.lithos.2008.09.010, 2009.

Wenk, H.-R. and Bulakh, A.: Minerals: their constitution and origin, Cambridge University Press, 646 pp., ISBN 0521529581, 2004.

Zeng, X., Joy, K. H., Li, S., Lin, Y., Wang, N., Li, X., Li, Y., Hao, J., Liu, J., and Wang, S.: Oldest immiscible silica-rich melt on the Moon recorded in a $\sim 4.38$ Ga zircon, Geophys. Res. Lett., 47, e2019GL085997, https://doi.org/10.1029/2019GL085997, 2020.

Zhang, R. Y., Liou J. G., and Lo, C.-H.: Raman spectra of polycrystalline microdiamond inclusions in zircons, and ultrahigh-pressure metamorphism of a quartzofeldspathic rock from the Erzgebirge terrane, Germany, Int. Geol. Rev., 59, 779–792, https://doi.org/10.1080/00206814.2016.1271366, 2017.